Title

Ion Diffusion Within Water Films in Unsaturated Porous Media

Journal

Environmental Science and Technology, 51(8)

ISSN

0013-936X

Authors

Tokunaga, Tetsu K

Finsterle, Stefan

Kim, Yongman

et al.

Publication Date

2017-04-18

DOI

10.1021/acs.est.6b05891

Peer reviewed

Environmental Science & Technology

Article

pubs.acs.org/est

Ion Diffusion Within Water Films in Unsaturated Porous Media

Tetsu K. Tokunaga,*[,†] Stefan Finsterle,[†] Yongman Kim,[†] Jiamin Wan,[†] Antonio Lanzirotti,[‡] and Matthew Newville[‡]

[†]Energy Geosciences Division, Lawrence Berkeley National Laboratory, Berkeley, California 94720, United States

[‡]Center for Advanced Radiation Sources, The University of Chicago, Chicago, Illinois 60637, United States

ABSTRACT: Diffusion is important in controlling local solute transport and reactions in unsaturated soils and geologic formations. Although it is commonly assumed that thinning of water films controls solute diffusion at low water contents, transport under these conditions is not well understood. We conducted experiments in quartz sands at low volumetric water contents (θ) to quantify ion diffusion within adsorbed films. At the lowest water contents, we employed fixed relative humidities to control water films at nm thicknesses. Diffusion profiles for Rb^+ and Br^- in unsaturated sand packs were measured with a synchrotron X-ray microprobe, and inverse modeling was used to determine effective diffusion coefficients, D_e, as low as $\sim 9 \times 10^{-15}$ m^2 s^{-1} at $\theta = 1.0 \times 10^{-4}$ m^3 m^{-3}, where the film thickness = 0.9 nm. Given that the diffusion coefficients (D_o) of Rb^+ and Br^- in bulk water (30 °C) are both $\sim 2.4 \times 10^{-9}$ m^2 s^{-1}, we found the impedance factor $f = D_e/(\theta D_o)$ is equal to 0.03 ± 0.02 at this very low saturation, in agreement with the predicted influence of interface tortuosity (τ_a) for diffusion along grain surfaces. Thus, reduced cross-sectional area (θ) and tortuosity largely accounted for the more than 5 orders of magnitude decrease in D_e relative to D_o as desaturation progressed down to nanoscale films.

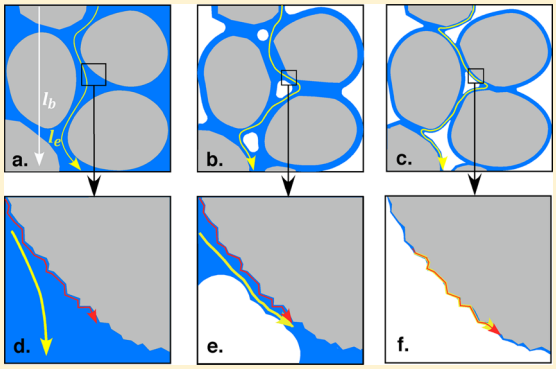

1. INTRODUCTION

The mobility of dissolved ions through the aqueous phase in soils and geological materials is important in a wide variety of processes including nutrient transport to plant roots and soil microorganisms,[1,2] the performance of barriers for subsurface waste isolation,[3,4] and electrical resistivity measurements employed in geophysical mapping of the subsurface.[5−7] Interest in these processes has motivated a large number of studies on diffusion of solutes in unsaturated as well as saturated soils and geologic media, summarized in comprehensive reviews.[8−11] The effective diffusion coefficient of a solute of interest in porous media, D_e, is of central importance in these numerous investigations, linking macroscopic diffusive fluxes, J, to gradients in their aqueous concentrations, C. For diffusion in response to a concentration gradient along the x-axis, Fick's Law gives J as

$$J = -D_e \frac{dC}{dx} \tag{1}$$

The magnitude of D_e depends on the diffusion coefficient of the species of interest in bulk water D_o, porosity n, volumetric water content θ, and tortuosity factor τ_o. Recognition of the controlling influence exerted by volumetric water content θ (the product of porosity n times water saturation S) and water film continuity goes back to early studies of solute diffusion in soils.[12−14] The pore network generally constrains solutes to diffuse along paths with effective lengths l_e that are longer than the bulk diffusion length l_b (Figure 1a), and these paths become longer as θ decreases (Figures 1b, c). Various definitions of tortuosity exist,[15] and here we use one convention of equating τ_o with $(l_b/l_e)^2$ such that τ_o decreases as θ decreases.[12,16] Diffusion within soils and geologic materials is sometimes further described as occurring not only through the aqueous phase in pores, but also via surface diffusion paths along water-mineral interfaces[17] (Figure 1d). Explanations for decreased magnitudes of D_e at low water contents include the constrictivity of very narrow paths, interactions with mineral surfaces, and increased water viscosity near these surfaces. These effects have also been included in models of diffusion in porous media.[12,18,19] While many porosity-saturation-tortuosity-constrictivity models have been developed to predict D_e,[9,20−23] independent quantification of individual factors is challenging. For simplicity, we will use the convention of expressing D_e as a reduction of D_o through two factors, θ and f[24]

$$D_e = f\theta D_o \tag{2}$$

Thus, the impedance factor f is equal to $D_e/(\theta D_o)$ and ranges from unity (for the limiting case of microscopically straight pathways with bulk fluid properties), down to zero (when solutes are immobilized through sorption and/or disconnected aqueous phases). $D_e/(\theta D_o)$ will be used later to assess the collective significance of all other factors besides θ (e.g., τ_o,

Received: November 22, 2016
Revised: February 27, 2017
Accepted: March 28, 2017
Published: March 28, 2017

DOI: 10.1021/acs.est.6b05891
Environ. Sci. Technol. 2017, 51, 4338−4346

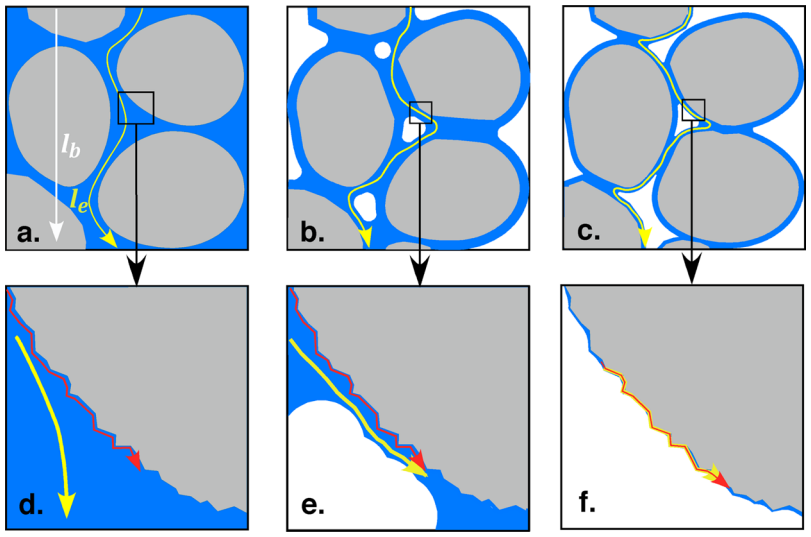

Figure 1. Conceptual illustrations of how solute diffusion pathways become more tortuous as the water content is decreased. Panels a–c show increased tortuosity in traversing multiple pores, with the greatest increases in path lengths expected during initial drainage, rather than with film thinning. Panels d–f show hypothetical diffusion pathways in bulk pore water (yellow) and along mineral surfaces (red), emphasizing the controlling role of water films when water saturation is low.

constrictivity, potentially increased viscosity, and increased interactions with interfaces) that contribute to decreased ion mobility as water saturation becomes very low.

It is worth noting for later discussion that the ratio $D_e/(\theta D_o) = f$ is the inverse of Saripalli et al.'s diffusion tortuosity factor τ_a, defined as the ratio of the air–water interfacial area in the unsaturated porous medium (a_{aw}) relative to that of an equivalent bundle of capillary tubes($a_{aw,o}$).[25] From the conceptual model presented in Figure 1, it is clear that the air–water interfacial area approaches the specific surface area of the solid phase at very low θ. Thus, at very low θ, f can be compared with the inverse of Saripalli et al.'s τ_a, with the air–water interfacial area equated with the specific surface area of the solid phase.

The vast majority of solute diffusion studies have been conducted in porous media at intermediate to high θ, typically in the range of about 0.1–0.5, which represent most soil and sediment environments. Some D_e measurements at $\theta < 0.1$ are available in the literature,[3,21,26−29] and low water saturations are common in (semi-) arid region soils and some deeper geologic formations including oil, gas, and geothermal reservoirs. In addition to their relevance in drier environments, measurements of D_e at low θ are needed for basic understanding of limiting conditions that allow transport via diffusion through the wetting fluid phase in unsaturated porous media, including the percolation threshold θ_{th} needed to permit diffusive transport.[23,30] Although models for solute diffusion can be categorized into those that implicitly allow diffusion coefficients to become infinitesimally small as water saturation approaches zero,[16,31] and those that consider a percolation threshold,[23,30,32] the lower limits of diffusion remain unclear.

Thinning of adsorbed water films has been invoked as the determinant for the lower limit of diffusion for ionic solutes because of their hydration and confinement between solid–water and water–gas interfaces.[12,29,32−34] This limit is expected when water film thicknesses approach dimensions of hydrated ion diameters. Given effective radii of ion hydration typically ranging from about 0.25–0.5 nm,[35] their diffusion appears feasible within water films at least as thin as 1 nm. Further constraints on ion mobility may result from strong interactions and ordering of water at mineral surfaces inferred from vapor adsorption energies, surfaces,[36−38] spectroscopic measurements,[37] and molecular dynamics (MD) simulations.[39] Indeed, the effective viscosity of water within the first two layers of the mineral surfaces has long been hypothesized to reduce ion mobility.[40,41] However, quasi-elastic neutron scattering measurements[42] and other MD simulations[43] indicate that mobilities of water and ions approach their bulk solution values rapidly beyond the first monolayer away from solid surfaces.[34,43,44]

Experimental tests of water and ion mobility along mineral water interfaces have typically been done in systems with moderate to high surface area.[32,40,41] The strong influence of surface area on the θ_{th} needed for diffusion has been well documented.[32,45] However, in order to isolate diffusion along adsorbed water films, it is useful to conduct studies in low θ systems where the complicating influences from water retained within clay interlayers[46] and in intragranular pores[47] are absent. To our knowledge, such experiments have not previously been conducted. Thus, this study focuses on solute diffusion in homogeneous quartz sands at low θ.

Examination of the lower limit of solute diffusion and its relation to water film thickness introduces several challenges in measurements and analyses. Tests require high spatial resolution or long experimental times in order to explore lower limits of diffusive transport. Moreover, for purposes of uniquely identifying the controlling role of adsorbed films, the relative fraction of water retained in intragranular pores and clay interlayers needs to be very small. These considerations led us to conduct unsaturated diffusion measurements on monodisperse quartz sands, conceptually illustrated in Figure 1. The required spatial resolution for measuring diffusion profiles was achieved through using a synchrotron X-ray fluorescence microprobe. Because of difficulties in homogeneously packing the sands, many of the diffusion profiles were found to be rather irregular and therefore best analyzed through inverse modeling.

DOI: 10.1021/acs.est.6b05891
Environ. Sci. Technol. 2017, 51, 4338–4346

2. MATERIALS AND METHODS

2.1. Sands. High purity quartz sands (total impurities <22 ppm) were obtained from the Quartz Corporation (Spruce Pine, NC). These sands were sieved to retain the 106−125 μm grain size fraction for use in the diffusion experiments. Specific surface areas determined by Kr-BET (Quantachrome Autosorb-1) were 0.069 ± 0.002 $m^2\ g^{-1}$, about 3.5 times greater than that of 110 μm diameter spheres of equivalent quartz density (2.65 g cm^{-3}).

2.2. Diffusion Cells and Sand Packing. The general approach used in all experiments was the half-cell method,[12,19] involving joining a sample containing the diffusion tracer (source half) to an identical sample initially lacking the tracer (sink half), then measuring concentration distributions along the joined system at a later time using a synchrotron X-ray fluorescence microprobe.[48,49] To facilitate accurate location of the interface between the two halves (x = 0) with the X-ray microprobe, anatase (TiO_2) powder was mixed into the source sand at 2.0 mg g^{-1} as a stationary label. RbBr was used as the diffusing tracer, initially present only in the source half. Either CsI or KI was added uniformly to both source and sink sands to provide a higher background concentration of relatively nonreactive ions in which Rb^+ and Br^- diffused. Experiments were conducted over two ranges of water contents: a low range from 4.0×10^{-3} to 5.0×10^{-2} g g^{-1} (6.6×10^{-3} to 8.2×10^{-2} $m^3\ m^{-3}$), and a partly overlapping ultralow range from 5.6×10^{-5} to 9.9×10^{-3} g g^{-1} (9.9×10^{-5} to 1.6×10^{-2} $m^3\ m^{-3}$). These different water content ranges required two different types of diffusion cells (Figure 2) and different approaches for establishing initial salt concentrations as described below.

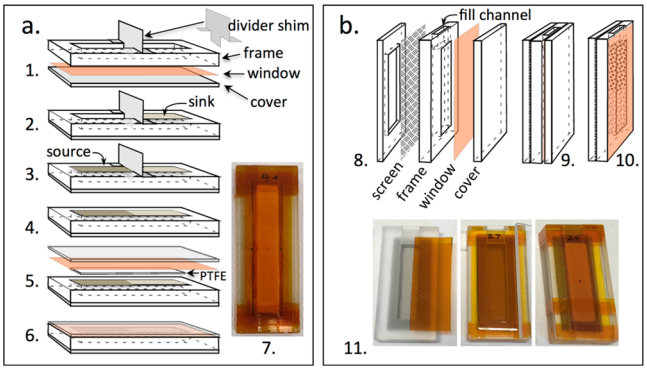

Figure 2. Diffusion cells. a. Low water content diffusion cell. 1. Open diffusion cell with divider shim in place, and window facing down. 2. Moist "sink" side sand packed. 3. Moist "source" side sand packed. 4. Shim removed. 5. Compaction of sand to final bulk density with PTFE back sheet, sealing with Kapton tape and back cover. 6. Assembled diffusion cell. 7. Photograph of diffusion cell with cover removed. b. Ultralow water content diffusion cell. 8. Exploded view of diffusion cell. 9. Assembled diffusion cell during filling with dry sand, and during diffusion with water films equilibrated with controlled humidity environment. 10. Diffusion cell with cover plate removed for X-ray microprobe measurements. 11. Photographs of diffusion cell (unassembled, assembled, sand-filled).

Low Water Content Systems. In these systems, separate solutions were prepared consisting of 1.5 M CsI for the sink half, and 50 mM RbBr with 1.5 M CsI for the source half. These solutions were added by pipet to their corresponding sink and source sands contained in individual scintillation vials, to achieve different water contents (4.0×10^{-3} to 5.0×10^{-2} g g^{-1}), quickly mixed with a spatula, and sealed with Al foil-line caps. The prewet samples were then stored for 2−8 days to allow more uniform distribution of water and solutes.

Each low water content diffusion cell consisted of a 6.35 mm thick acrylic sample frame to contain a 10 mm wide, 60 mm long diffusion region (30 mm long half-cells) with a 50 μm thick X-ray transparent polyimide (Kapton) window (Figure 2a). With the window and supporting cover sealed onto the bottom side of the frame, a stainless steel divider shim was secured at the midplane of the diffusion cell, and 2.35 g (equivalent dry mass of premoistened sand) of tracer-free sand was distributed within the cell on one side of the divider. The opposite side of the diffusion cell was filled with the same mass of tracer-containing sand (same water content). After leveling the sands on each side, the divider was removed, and a 10 × 60 × 0.16 mm thick PTFE (Telfon) sheet was pressed onto the sand and into the frame. Compression of the sands by the PTFE sheet facilitated contact between the two sand regions and established time zero for diffusion. With the upper surface of the PTFE sheet level with that of the acrylic frame, the sand was compressed to a bulk density of 1.64 g cm^{-3} (total porosity = 0.38). The PTFE backing was secured to the frame with Kapton tape and additional acrylic support plate, and stored in a high humidity (>99%) chamber at laboratory room temperature (23 ± 1 °C). Two days prior to X-ray microprobe measurements of diffusion profiles, these diffusion cells were doubly contained in humidified (moistened towels) plastic bags for shipment to the Advanced Photon Source at Argonne National Laboratory.

Ultralow Water Content Systems. For the driest sands, water contents were established by equilibration with fixed relative humidity (rh) environments which were controlled with saturated salt solutions.[50] Although water vapor adsorption isotherms were determined on the sand for rh values ranging from 0.077 up to 0.97 (97%),[51] diffusion profiles were only obtained on a subset of rh values ranging from 0.216 up to 0.923 because of disturbance of the contact plane in some of the cells described later. In order to minimize temperature variations in controlled humidity environments, adsorption isotherms and diffusion sample incubations were conducted in an incubator at 30.0 ± 0.5 °C. Sands for the source sides were prepared by first mixing in the inert TiO_2 as described previously, then wetting with a solution consisting of up to 200 mM KI and 5.0 mM RbBr (lower concentrations added to sands to be maintained at rh <0.22) to an initial water content of 6.0×10^{-2} g g^{-1}. Sands for the sink sides of diffusion cells were prepared without TiO_2, and spiked only with KI (same ionic strength as applied to the source side, solution/sand = 6.0×10^{-2} g g^{-1}). After spiking and thoroughly mixing solutions in each sink/source sand batch, sands were dried overnight at 60 °C, cooled to room temperature in a desiccator, and then each sample was further mixed prior to packing into a diffusion cell.

Each ultralow water content diffusion cell consisted of a 6.35 mm thick acrylic sample frame to contain a 10 mm wide, 40 mm long diffusion region (20 mm long half-cells), 50 μm thick X-ray transparent polyimide (Kapton) window, and a 160-mesh stainless steel screen backing to allow rapid adsorption of water vapor (Figure 2b). The assembled diffusion cell was vertically oriented, filled through the top channel with the dry "sink" sand up to the midplane (20 mm) in ∼5 mm increments, and each increment lightly compacted to achieve a bulk density of 1.64 g cm^{-3}. The remaining volume was similarly filled with the RbBr- and TiO_2-containing dry sand, and the access port was sealed

DOI: 10.1021/acs.est.6b05891
Environ. Sci. Technol. 2017, 51, 4338−4346

Table 1. Water Vapor Adsorption Isotherms for Quartz Sand, 106-125 μm, at 30 °C, Comparing Sands without Salts, And with KI and RbBr Salts[a]

saturated salt solution for controlling rh	relative humidity (30 °C)	washed sand		sand with KI, RbBr salt	
		water content, g g^{-1}	water film thickness, nm	water content, g g^{-1}	water film thickness, nm
LiBr	0.077	2.6×10^{-5}	0.34	3.0×10^{-5}	0.43
LiCl	0.113	3.7×10^{-5}	0.60	4.4×10^{-5}	0.55
K-acetate	0.216*	5.4×10^{-5}	0.79	5.6×10^{-5}	0.81
$MgCl_2 \bullet 6H_2O$	0.324*	5.6×10^{-5}	0.90	6.8×10^{-5}	0.98
NaBr	0.560	6.4×10^{-5}	1.2	7.6×10^{-5}	1.1
NaCl	0.751*	7.5×10^{-5}	1.4	1.6×10^{-3}	23
KCl	0.836*	8.2×10^{-5}	1.7	5.0×10^{-3}	72
KNO_3	0.923*	2.1×10^{-4}	2.8	9.9×10^{-3}	143
K_2SO_4	0.970	3.3×10^{-4}	7.0		

[a]Conditions associated with diffusion measurements are indicated by asterisks.

with an acrylic plug. The ultralow water content diffusion cells were placed on support plates in separate desiccator jars containing the different saturated salt solutions listed in Table 1 for 28−38 days at 30 °C. Two days prior to X-ray measurements, the individual diffusion cells were sealed in plastic bags containing paper towels wet with their corresponding saturated salt solutions, and shipped to the synchrotron facility.

2.3. X-ray Fluorescence Microprobe Measurements of Diffusion Profiles. High-resolution diffusion profiles in a variety of materials are obtainable with a synchrotron X-ray fluorescence microprobe.[52,53] The synchrotron X-ray fluorescence microprobe at beamline 13-ID-E, at the Advanced Photon Source, Argonne National Laboratory was operated with a monochromatic beam energy of 17.00 keV, with a spot size of 5 μm (vertical) by 500 μm (horizontal). This beam geometry allowed quick mapping of the vertically oriented diffusion cells with high spatial resolution along the diffusion direction while averaging over multiple sand grains orthogonal to this axis. A four element Vortex ME-4 silicon drift detector was used to map distributions of Ti K_α (4.511 keV) and the combined (overlapped) Br K_β (13.291 keV) and Rb K_α (13.395 keV) regions of interest (referred to simply as Rb). The sample was rastered continuously across the stationary beam, and X-ray fluorescence spectra were collected in continuous scanning mode, typically with 100 μm horizontal, and 50 μm vertical pixels, and 0.1 s/pixel. Maps were typically collected within a 6−8 mm wide strip, spanning from 20 to 60 mm in length along the diffusion direction, within about 1 h. One-dimensional diffusion profiles were obtained by averaging fluorescence intensities along the direction transverse to diffusion.

D_e from Analytical Solution. When both the source half ($x < 0$, initially at concentration C_o) and sink half ($x > 0$, initially at concentration zero) of the diffusion cell are identical with respect to their θ and D_e, the diffusion profile is described by

$$\frac{C}{C_o} = \frac{1}{2}\mathrm{erfc}\left(\frac{x}{2\sqrt{D_e t}}\right) \quad (3)$$

over times short enough that concentrations at external boundaries remain unchanged.[54] The measured diffusion profiles revealed that uniform column packing was usually not achieved, motivating analyses through inverse modeling.

2.4. Inverse Modeling to Determine D_e. The 60 and 40 mm long diffusion cells were modeled as one-dimensional porous materials. The domain was discretized into 0.05 mm long elements, that is, at a resolution identical to the Rb concentration data. Rb transport is modeled as a Fickian diffusion process in the liquid phase only, that is, advective transport or multiphase diffusion effects are ignored. The model domain is divided in two halves, the left representing the Rb source zone, and the right the Rb sink zone. For modeling the low water content systems, the source and sink zones are separated by three grid blocks (i.e., a 0.15 mm wide zone) at the center of the diffusion cell. This zone represents the location of the removed divider, where the material may be disturbed and water films may have reduced contact compared to that in the undisturbed zones. Each of these three zones is allowed to have its own tortuosity factor used to calculate D_e. Subdividing the experiment into three regions is motivated by the different treatments they underwent during sample preparation. While the thickness of the zone disturbed by the divider is unknown, an error in the assumed thickness will only affect the estimated diffusion coefficient of the disturbed zone, which is of no interest. Moreover, the assumption that the source and sink zones are essentially homogeneous appears justified by the fact that no distinct change in diffusion behavior is evident from the measured concentration profiles, and that no discrete changes in the residuals can be observed after calibration. Minimizing the number of regions (and thus number of parameters to be estimated) is desirable to avoid overparameterization of the inverse problem, which would lead to strong parameter correlations and consequently large estimation uncertainties. In these calculations, $n = 0.38$, θ and S are set to their cell-specific values, and D_o is set to 2.1×10^{-9} and 2.4×10^{-9} m^2 s^{-1}, at 23.0 and 30.0 °C, respectively.[19,55] Water contents in the source and sink halves of the cell are initialized as measured; they do not change during the simulation. Normalized Rb concentrations on the left and right are set to 1.0 and 0.0, respectively. The simulations were performed using the TOUGH2 simulator,[56] with runs continued to the times corresponding to when the Rb profiles were measured with the X-ray microprobe. The main processes being simulated are multicomponent molecular diffusion under a local thermodynamic equilibrium assumption; advection was inhibited by specifying a permeability of zero. Each measured data point was included in the inversion. Measurement errors were assumed heteroscedastic, with $\sigma_c = 0.02c + 0.01$, where c is the measured normalized Rb concentration (i.e., $c = C/C_o$).

DOI: 10.1021/acs.est.6b05891
Environ. Sci. Technol. 2017, 51, 4338−4346

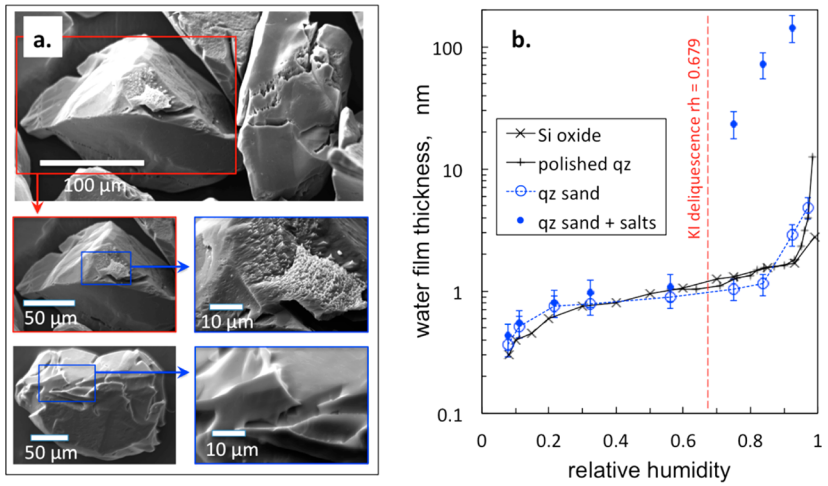

Figure 3. Quartz sands and water films associated with the ultralow water content diffusion experiments. a. Scanning electron micrographs of sands. b. Water vapor adsorption isotherms, comparing measurements on sands with isotherms from the literature[37,59] obtained on flat silica surfaces. Influences of the KI and RbBr salts added to sands become significant above the deliquescence rh of KI.

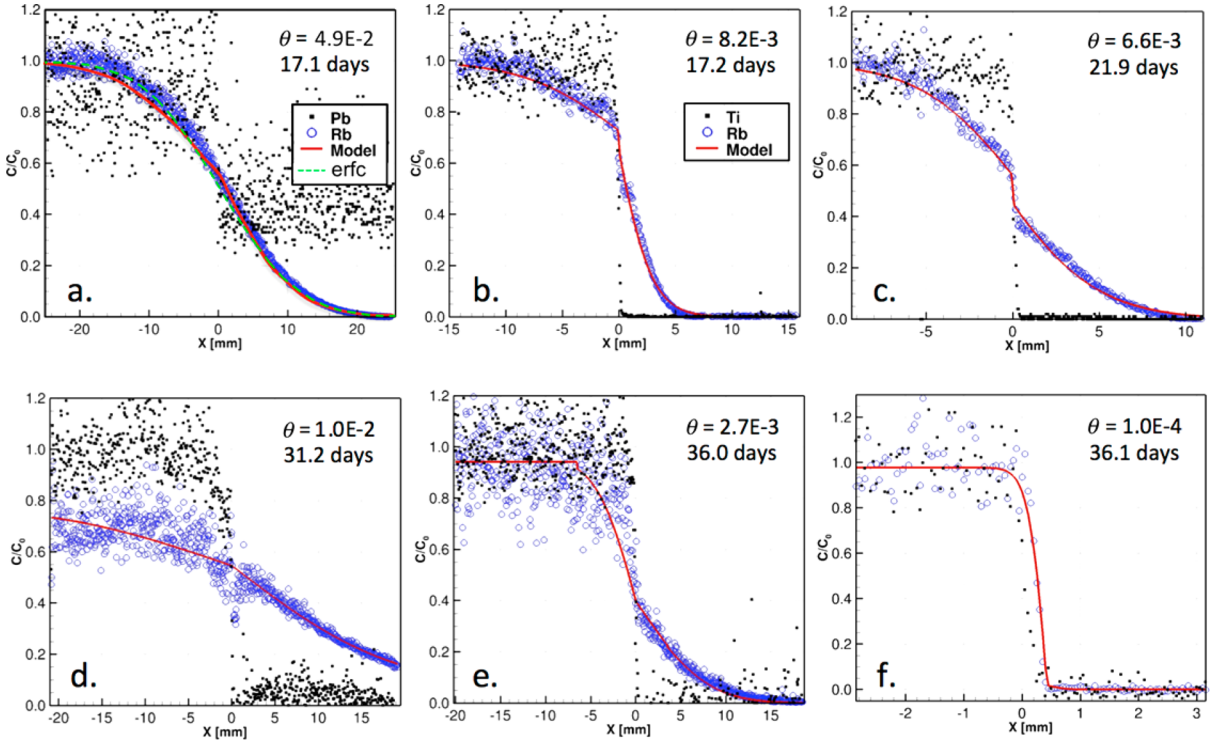

Figure 4. Example diffusion profiles from the low water content (**a-c**) and ultralow water content systems (d–f).

The weighted least-squares objective function was minimized using the Levenberg–Marquardt algorithm as implemented in iTOUGH2.[57,58]

3. RESULTS AND DISCUSSION

3.1. Adsorption Isotherms and Water Film Thicknesses. The saturated salt solutions, rh, gravimetric water contents, and water film thicknesses are shown in Table 1 for two substrates, clean washed sands and sands containing KI and RbBr at levels used to spike the source half of the ultralow water content systems. Although the surfaces of the sand have rough microtopography (Figure 3a), the low specific surface area (0.069 $m^2\ g^{-1}$) indicates that intragranular uptake of water was insignificant. Thus, at low water contents, water resides largely as adsorbed films on grain surfaces and to lesser extent as pendular rings around grain–grain contact points. Adsorption isotherms similar to that obtained on the washed sands have been previously reported on flat Si-oxide and quartz surfaces,[37,59] indicating that capillary condensation in the sand's rough surfaces was minor. Water vapor adsorption isotherms for the salt-spiked sands exhibited two distinct regions delineated by the deliquescence relative humidity of the dominant salt, KI (rh 0.68 at 30.0 °C[50]). Below this rh, water film thicknesses on the salt-treated sands were experimentally indistinguishable from values obtained in the washed (salt-free) sands. In contrast, hydration and dissolution of KI resulted in much greater water film thicknesses in the salt-treated sands (Figure 3b). The extent of film thickness increase was also

DOI: 10.1021/acs.est.6b05891
Environ. Sci. Technol. 2017, 51, 4338–4346

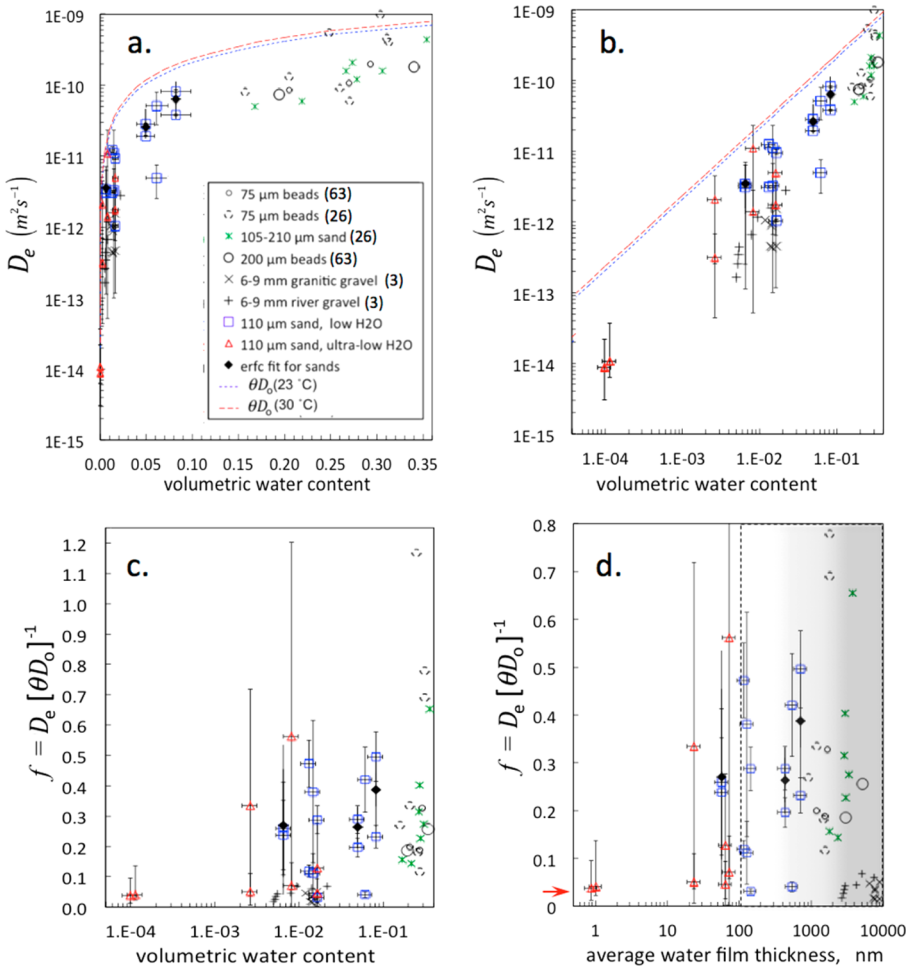

Figure 5. Influence of water content and water film thickness on diffusion, comparing results of this study with literature values. a, b. D_e versus θ (with θ plotted linearly and logarithmically in a and b, respectively). Numbers included in the legend refer to literature sources.[3,26,66] The dashed lines represent θD_o, and denote upper limits of D_e when $f = 1$. D_o was set equal to 2.0×10^{-9} and 2.4×10^{-9} m^2 s^{-1} at 23.0 and 30.0 °C, respectively. c. Impedance factor versus volumetric water content. d. Impedance factor versus water film thickness. The red arrow indicates the predicted $f = 0.03$in the thin film limit. The region with average water films >100 nm (outlined and shaded region in 5d) have significant contributions from capillary water.

influenced by the variable initial water/sand mass ratio achieved (4.0×10^{-3} to 5.0×10^{-2} g g^{-1}) upon adding the KI solution. It should be noted that water vapor adsorption equilibrium times ranged from ~0.2 days (rh <0.33) to 2 days (rh = 0.923).

3.2. Measured Diffusion Profiles and Calculated D_e. Examples of normalized Rb diffusion profiles and matches obtained with the calibrated models are shown in Figure 4. The measured data are shown as blue symbols (individual points are averages of eight values obtained at a specific x position, with coefficients of variation typically ranging from 0.1 to 0.2), and the simulated concentration profiles are represented by solid red lines. Also shown in these graphs are normalized profiles for the inert Ti tracer used to locate the internal midplane boundary. It should be noted that collection of the Ti K_α profile was unsuccessful on one of the wettest systems (Figure 4a). However, Pb is a common impurity in anatase,[60,61] and the Pb L_α (10.552 keV) profile exhibited a distinct step that allowed identification of the midplane location. The Ti and Pb profiles not only located the midplane position in each cell, but also helped determine if the integrity of each cell was suitable for obtaining diffusion measurements. Several of the cells did not exhibit sharp steps in Ti profiles, indicating mechanical disturbance of the sands. These cells were excluded from diffusion analyses.

The measured diffusion profiles were commonly asymmetric about the midplane (e.g., Figures 4b–d), indicative of differences in packing between the source and sink sections. Lower packing density at the interface region in some of the low water content systems is also evident from very steep Rb concentration gradients at the midplane (Figure 4b,c). Only a few of the cells exhibited symmetric diffusion profiles amenable to approximation as a homogeneous medium. The diffusion profile obtained by fitting eq 3 to the normalized Rb profile is indicated by the dashed green line in Figure 4a, where the fit D_e of 2.59×10^{-11} m^2 s^{-1} (root-mean-square difference in concentration = 0.031) is between values obtained with TOUGH2 for the source and sink sides of the cell (2.84×10^{-11} and 1.93×10^{-11} m^2 s^{-1}, respectively).

The D_e values obtained via inverse modeling of the diffusion profiles (and a few D_e from fitting eq 3) are summarized in Figure 5a and b, with a logarithmic x axis used in the latter graph to facilitate examination of trends at very low θ. Included in this graph are literature D_e values of other coarse-textured media that were expected to have negligible intragranular porosity, such that diffusion at low saturations would be

DOI: 10.1021/acs.est.6b05891
Environ. Sci. Technol. 2017, 51, 4338–4346

restricted to occur through adsorbed water films. Results of our measurements and calculations are in agreement with the general trend of decreasing D_e with decreasing θ, and to our knowledge extend the lower limits of measured solute diffusion in unsaturated media substantially lower than previous studies. Included in Figure 5a and b are lines representing θD_o, for nominal room temperature (23 °C) and for 30 °C. Note that the D_e values generally reside within a moderately narrow, θ-dependent band below the θD_o lines. Our experiments at the lowest θ of 9.9×10^{-5} and 1.1×10^{-4} yielded D_e of 8.7×10^{-15} and 1.1×10^{-14} m^2 s^{-1}, respectively.

The dominant influence of θ on D_e becomes more apparent when considering the impedance factor f, obtained by dividing the D_e values by their associated θD_o. These $D_e/(\theta D_o)$ are plotted with respect to θ in Figure 5c. Note that over more than 3 orders of magnitude variation in θ, the f values vary only moderately, largely in the range between 0.02 and 0.5. These f values are replotted with respect to water film thickness in Figure 5d. For our quartz sands, measured θ were divided by the product of bulk density (1.64 g cm^{-3}) times the specific surface area (0.069 m^2 g^{-1}) to obtain values of average film thicknesses. For the other granular materials from the literature, their median diameters were selected, and specific surface areas were estimated as being 3.5 times that of spheres of these median diameters (3.5 being the ratio of BET-measured surface area of our sand relative to the smooth sphere equivalent surface area). These estimated surface areas were then used with the reported θ and bulk density values to estimate film thicknesses. From Figures 5c and d, it is evident that $f \sim 0.3 \pm 0.2$ describe a wide range of θ as well as average film thicknesses, and that $f = 0.03 \pm 0.02$ for the lowest measured θ. From Figure 5d, we see that the diffusion of Rb^+ and Br^- in our driest systems (rh = 0.216 and 0.324) takes place via 0.9−1.0 nm thick films, with mobility similar to that associated with much thicker films. Thus, for unreactive ions, tortuosity by itself accounts for diffusive transport reduction in water films as thin as 0.9 nm, without appreciable retardation attributable to putative increases in viscosity.

Recall that in the limit of very low θ, the air−water interfacial areas in our systems approaches the specific surface area of the sand, so that the f for diffusion along ~1 nm water films can be compared to predictions based on the tortuosity model developed by Saripalli et al.[25] On a volumetric basis, this surface area denoted a_{aw} is the product of the surface area per unit mass (0.069 m^2 g^{-1}) times the bulk density (1.64 g cm^{-3}), and equals 1.13×10^6 m^{-1}. Calculating the volume-based surface area of an equivalent bundle of capillary tubes requires defining a characteristic drained capillary radius, r. For this purpose, we note that drainage of monodisperse sands occurs at a distinct capillary pressure P_c predictable from grain size (λ), air−water interfacial tension (γ), and the scale drainage inflection capillary pressure (Π_c) by[62−64]

$$P_c = \gamma \prod_c / \lambda \tag{4}$$

With $\Pi_c = 12$, $\gamma = 0.073$ N m^{-1}, and $\lambda = 110$ μm, the P_c at the drainage inflection point is 8.0 kPa. From the Young−Laplace equation,

$$P_c = 2\gamma / r \tag{5}$$

which leads to

$$r = 2\lambda / \prod_c = \lambda / 6 \tag{6}$$

Thus, $r \sim 18$ μm for our 110 μm sand. Following Saripalli et al.,[25] in the limit of very low θ, surface area per unit volume in the reference capillary tube bundle is

$$a_{aw,o} = 2n/r = 4.1 \times 10^4 m^{-1} \tag{7}$$

Thus, $\tau_a = a_{aw}/a_{aw,o} = 28$, and the tortuosity model predicted $f = \tau_a^{-1} = 0.036$ in the thin film limit indicated by the red arrow on the y-axis of Figure 5d agrees well with results obtained on the two driest sands. This agreement, combined with the relatively small variation in f over orders of magnitude changes in water content, indicate that interactions with interfaces did not strongly retard diffusion of Rb^+ and Br^-, even in 0.9 nm films.

It should be noted that films greater than about 100 nm in the shaded region of Figure 5d exceed thicknesses strictly attributable to adsorption,[65] and include significant contributions from capillarity at grain contacts, surface roughness, and potentially intragranular pores. We do not have an explanation for the rather wide variation in f measured over most of our tested θ, but note that similarly wide ranges in $f(\theta)$ are typical of the data in the earlier literature as well (Figures 5c,d).

4. IMPLICATIONS FOR DIFFUSION IN THIN FILMS

Measurements of Rb^+ and Br^- diffusion within adsorbed water films spanning 2 orders of magnitude in thickness (from about 100 nm down to 1 nm) were obtained through experiments in unsaturated, monodisperse, pure quartz sands. The limited reduction in the impedance factor f over a wide range in film thicknesses is consistent with some previous experimental[42] and computational[34,43] investigations that found only minor decreases in mobility of ions and water near solid surfaces. However, other studies involving clays and nanoscale fractures have reported more substantial decreases in water and ion mobility.[39−41] Further tests are needed to determine the extent to which these contrasting conclusions reflect differences in confining environments; confinement between opposing solid−water interfaces of nanofractures and clay interlayers, versus adsorbed films bounded by solid−water and water−gas interfaces. In addition, experiments involving other cation−anion pairs having distinctly different hydrated radii and mineral surface interactions will be useful for better understanding mobility along interfaces. The approach developed here involving humidity control will be useful for further investigations of transport in adsorbed water films, particularly in the nm and subnm thickness range.

AUTHOR INFORMATION

Corresponding Author

*Phone 510-486-7176; fax: 510-486-5686; e-mail: tktokunaga@lbl.gov.

ORCID

Tetsu K. Tokunaga: 0000-0003-0861-6128

Notes

The authors declare no competing financial interest.

ACKNOWLEDGMENTS

TKT and JW dedicate this paper to Garrison Sposito (recently retired[67]), with gratitude for his inspirational science and teaching. This material is based upon work supported by the U.S. Department of Energy, Office of Science, Office of Basic

DOI: 10.1021/acs.est.6b05891
Environ. Sci. Technol. 2017, 51, 4338−4346

Energy Sciences, Chemical Sciences, Geosciences, and Biosciences Division under contract number DE-AC02-05CH11231. Portions of this work were performed at GeoSoilEnviroCARS (The University of Chicago, Sector 13), Advanced Photon Source, Argonne National Laboratory. GeoSoilEnviroCARS is supported by the National Science Foundation - Earth Sciences (EAR-1128799) and Department of Energy- Geosciences (DE-FG02-94ER14466). This research used resources of the Advanced Photon Source, a U.S. Department of Energy (DOE) Office of Science User Facility operated for the DOE Office of Science by Argonne National Laboratory under Contract No. DE-AC02-06CH11357. We thank Dr. Tony Asbridge and The Quartz Corporation for providing samples of NC4A quartz sand, Wenming Dong (LBNL) for BET measurements, Steve Ferreira (LBNL) for machining the diffusion cells, and the anonymous reviewers for their helpful comments.

REFERENCES

(1) Holden, P. A.; Fierer, N. Microbial processes in the vadose zone. *Vadose Zone J.* **2005**, *4*, 1−21.
(2) Long, T.; Or, D. Aquatic habitats and diffusion constraints affecting microbial coexistence in unsaturated porous media. *Water Resour. Res.* **2005**, *41* (8), W08408.
(3) Conca, J. L.; Wright, J. Diffusion-coefficients in gravel under unsaturated conditions. *Water Resour. Res.* **1990**, *26* (5), 1055−1066.
(4) Jansik, D. P.; Wildenschild, D.; Rosenberg, N. D. Flow processes in the dry regime: The effect on capillary barrier performance. *Vadose Zone J.* **2011**, *10* (4), 1173−1184.
(5) Ewing, R. P.; Hunt, A. G. Dependence of the electrical conductivity on saturation in real porous media. *Vadose Zone J.* **2006**, *5* (2), 731−741.
(6) Kumar, M.; Senden, T. J.; Sheppard, A. P.; Arns, C. H.; Knackstedt, M. A. Probing the Archie's Exponent under Variable Saturation Conditions. *Petrophysics* **2011**, *52* (2), 124−134.
(7) Hunt, A. G. Continuum percolation theory and Archie's law. *Geophys. Res. Lett.* **2004**, *31* (19), L19503.
(8) Shackelford, C. D. Laboratory diffusion testing for waste disposal-A review. *J. Contam. Hydrol.* **1991**, *7*, 177−217.
(9) Hu, Q. H.; Wang, J. S. Y. Aqueous-phase diffusion in unsaturated geologic media: A review. *Crit. Rev. Environ. Sci. Technol.* **2003**, *33* (3), 275−297.
(10) Bourg, I. C.; Bourg, A. C. M.; Sposito, G. Modeling diffusion and adsorption in compacted bentonite: a critical review. *J. Contam. Hydrol.* **2003**, *61* (1−4), 293−302.
(11) Appelo, C. A. G. *A Review of Porosity and Diffusion in Bentonite; Posiva* **2013**, 36.
(12) Porter, L. K.; Kemper, W. D.; Jackson, R. D.; Stewart, B. A. Chloride diffusion in soils as influenced by moisture content. *soil Science Society of America Proceedings* **1960**, *24*, 460−463.
(13) Stewart, B. A.; Eck, H. V. The movement of surface-applied nitrate into soils at five moisture levels. *Soil Science Society America Proceedings* **1958**, *22* (3), 260−262.
(14) Brown, D. A. Cation exchange in soils through the moisture range, saturation to the wilting percentage. *Soil Science Society of America Proceedings* **1953**, *17* (2), 92−96.
(15) Ghanbarian, B.; Hunt, A. G.; Ewing, R. P.; Sahimi, M. Tortuosity in porous media: A critical review. *Soil Science Society of America Journal* **2013**, *77* (5), 1461−1477.
(16) Papendick, R. I.; Campbell, G. S., Theory and measurement of water potential. In *Water Potential Relations in Soil Microbiology*; Parr, J. F.; Gardner, W. R.; Elliott, L. F., Eds.; Soil Science Society of America: Madison, WI, 1981; pp 1−22.
(17) Oscarson, D. W. Surface diffusion: Is it an important transport mechanism in compacted clays? *Clays Clay Miner.* **1994**, *42* (5), 534−543.
(18) van Brakel, J.; Heertjes, P. M. Analysis of diffusion in macroporous media in terms of a porosity, a tortuosity and a constrictivity factor. *Int. J. Heat Mass Transfer* **1974**, *17* (9), 1093−1103.
(19) Flury, M.; Gimmi, T. F., Solute diffusion. In *Methods of Soil Analysis, Part 4, Physical Methods*, Dane, J. H.; Topp, G. C., Eds.; Soil Science Society of America: Madison, WI, 2002; pp 1323−1351.
(20) Lim, P. C.; Barbour, S. L.; Fredlund, D. G. The influence of degree of saturation on the coefficient of aqueous diffusion. *Can. Geotech. J.* **1998**, *35* (5), 811−827.
(21) Chou, H.; Wu, L.; Zeng, L.; Chang, A. Evaluation of solute diffusion tortuosity factor models for variously saturated soils. *Water Resour. Res.* **2012**, *48*, WR011653.
(22) Moldrup, P.; Olesen, T.; Blendstrup, H.; Komatsu, T.; de Jonge, L. W.; Rolston, D. E. Predictive-descriptive models for gas and solute diffusion coefficients in variably saturated porous media coupled to pore-size distribution: IV. Solute diffusivity and the liquid phase impedance factor. *Soil Sci.* **2007**, *172* (10), 741−750.
(23) Hunt, A. G.; Ghanbarian, B.; Ewing, R. P., Saturation Dependence of Solute Diffusion in Porous Media: Universal Scaling Compared with Experiments. *Vadose Zone J.* **2014**, *13* (4). doi:010.2136/vzj2013.12.0204.
(24) Nye, P. H.; Tinker, P. B. *Solute Movement in the Soil-Root System*; University of California Press: Berkeley, 1977; p 342.
(25) Saripalli, K. P.; Serne, R. J.; Meyer, P. D.; McGrail, B. P. Prediction of diffusion coefficients in porous media using tortuosity factors based on interfacial areas. *Groundwater* **2002**, *40* (4), 346−352.
(26) Romkens, M. J. M.; Bruce, R. R. Nitrate diffusivity in relation to moisture content of non-adsorbing porous media. *Soil Sci.* **1964**, *98* (5), 332−337.
(27) Mehta, B. K.; Shiozawa, S.; Nakano, M. Measurement of molecular diffusion of salt in unsaturated soils. *Soil Sci.* **1995**, *159* (2), 115−121.
(28) Heller, P.; Wright, J. *The Determination of Diffusion Coefficient of Invert Materials, Civilian Radioactive Waste Management System Management & Operating Contractor*, TDR-EBS-MD-000002 REV 00; U.S. Department of Energy, Yucca Mountain Site Characterization Office: Richland, WA, January 18, 2000, 2000.
(29) Hu, Q. H.; Kneafsey, T. J.; Roberts, J. J.; Tomutsa, L.; Wang, J. S. Y. Characterizing unsaturated diffusion in porous tuff gravel. *Vadose Zone J.* **2004**, *3* (4), 1425−1438.
(30) Revil, A.; Jougnot, D. Diffusion of ions in unsaturated porous materials. *J. Colloid Interface Sci.* **2008**, *319* (1), 226−235.
(31) Millington, R.; Quirk, J. P. Permeability of porous solids. *Trans. Faraday Soc.* **1961**, *57* (8), 1200.
(32) Olesen, T.; Moldrup, P.; Henriksen, K.; Petersen, L. W. Modeling diffusion and reaction in soils 0.4. New models for predicting ion diffusivity. *Soil Sci.* **1996**, *161* (10), 633−645.
(33) Martys, N. S. Diffusion in partially-saturated porous materials. *Mater. Struct.* **1999**, *32* (222), 555−562.
(34) Churakov, S. V. Mobility of Na and Cs on montmorillonite surface under partially saturated conditions. *Environ. Sci. Technol.* **2013**, *47* (17), 9816−9823.
(35) Marcus, Y. Effect of Ions on the Structure of Water: Structure Making and Breaking. *Chem. Rev.* **2009**, *109* (3), 1346−1370.
(36) Parks, G. A. Surface and interfacial free-energies of quartz. *Journal of Geophysical Research* **1984**, *89* (Nb6), 3997−4008.
(37) Asay, D. B.; Kim, S. H. Evolution of the adsorbed water layer structure on silicon oxide at room temperature. *J. Phys. Chem. B* **2005**, *109* (35), 16760−16763.
(38) Barshad, I. In *Adsorptive and Swelling Properties of Clay-Water Systems*, First National Conference on Clays and Clay Technology, Berkeley, 1955, 1952; California Division of Mines: Berkeley, 1952; pp 70−77.
(39) Kerisit, S.; Liu, C. X. Molecular simulations of water and ion diffusion in nanosized mineral fractures. *Environ. Sci. Technol.* **2009**, *43* (3), 777−782.
(40) Kemper, W. D. Water and ion movement in thin films as influenced by electrostatic charge and diffuse layer of cations

DOI: 10.1021/acs.est.6b05891
Environ. Sci. Technol. 2017, 51, 4338−4346

associated with clay mineral surfaces. *Soil Science Society America Proceedings* **1960**, *24*, 10−16.
(41) Kemper, W. D.; Maasland, D. E. L.; Porter, L. K. Mobility of water adjacent to mineral surfaces. *Soil Science Society America Proceedings* **1964**, *28* (3), 164−167.
(42) Takahara, S.; Sumiyama, N.; Kittaka, S.; Yamaguchi, T.; Bellissent-Funel, M. C. Neutron scattering study on dynamics of water molecules in MCM-41. 2. Determination of translational diffusion coefficient. *J. Phys. Chem. B* **2005**, *109* (22), 11231−11239.
(43) Bourg, I. C.; Steefel, C. I. Molecular dynamics simulations of water structure and diffusion in silica nanopores. *J. Phys. Chem. C* **2012**, *116* (21), 11556−11564.
(44) Kulasinski, K.; Guyer, R.; Derome, D.; Carmeliet, J. Water diffusion in amorphous hydrophilic systems: A stop and go process. *Langmuir* **2015**, *31* (39), 10843−10849.
(45) Moldrup, P.; Olesen, T.; Komatsu, T.; Schjonning, P.; Rolston, D. E. Tortuosity, diffusivity, and permeability in the soil liquid and gaseous phases. *Soil Sci. Soc. Am. J.* **2001**, *65* (3), 613−623.
(46) Bourg, I. C.; Sposito, G.; Bourg, A. C. M. Modeling the diffusion of Na+ in compacted water-saturated Na-bentonite as a function of pore water ionic strength. *Appl. Geochem.* **2008**, *23* (12), 3635−3641.
(47) Tokunaga, T. K.; Olson, K. R.; Wan, J. Moisture Characteristics of Hanford Gravels: Bulk, Grain-Surface, and Intragranular Components. *Vadose Zone J.* **2003**, *2* (3), 322−329.
(48) Newville, M.; Sutton, S.; Rivers, M.; Eng, P. Micro-beam X-ray absorption and fluorescence spectroscopies at GSECARS: APS beamline 131D. *J. Synchrotron Radiat.* **1999**, *6*, 353−355.
(49) Tokunaga, T.; Wan, J.; Pena, J.; Sutton, S.; Newville, M. Hexavalent uranium diffusion into soils from concentrated acidic and alkaline solutions. *Environ. Sci. Technol.* **2004**, *38* (11), 3056−3062.
(50) Greenspan, L. Humidity fixed-points of binary saturated aqueous-solutions. *J. Res. Natl. Bur. Stand., Sect. A* **1977**, *81* (1), 89−96.
(51) Tokunaga, T. K.; Olson, K. R.; Wan, J. M. Moisture characteristics of Hanford gravels: Bulk, grain-surface, and intragranular components. *Vadose Zone J.* **2003**, *2* (3), 322−329.
(52) Koepke, J.; Behrens, H. Trace element diffusion in andesitic melts: An application of synchrotron X-ray fluorescence analysis. *Geochim. Cosmochim. Acta* **2001**, *65* (9), 1481−1498.
(53) Tokunaga, T. K.; Wan, J.; Pena, J.; Sutton, S. R.; Newville, M. Hexavalent uranium diffusion into soils from concentrated acidic and alkaline solutions. *Environ. Sci. Technol.* **2004**, *38*, 3056−3062.
(54) Crank, J. *The Mathematics of Diffusion*, 2nd ed.; Clarendon: Oxford, 1975; p 415.
(55) Robinson, R. A.; Stokes, R. H. *Electrolyte Solutions*. 2nd ed.; Academic Press: New York, 1959; p 559.
(56) Pruess, K.; Oldenburg, C.; Moridis, G. *TOUGH2 User's Guide. Version 2.1*; Lawrence Berkeley National Laboratory: Berkeley, CA, 2012; p 210.
(57) Finsterle, S.; Commer, M.; Edmiston, J. K.; Jung, Y.; Kowalsky, M. B.; Pau, G. S. H.; Wainwright, H. M.; Zhang, Y., iTOUGH2: A simulation-optimization framework for analyzing multiphysics subsurface systems. *Comput. Geosci.* **2016**, *in press*, http://dx.doi.org/10.1016/j.cageo.2016.09.005i.10.1016/j.cageo.2016.09.005
(58) Finsterle, S. Multiphase inverse modeling: Review and iTOUGH2 applications. *Vadose Zone J.* **2004**, *3* (3), 747−762.
(59) Gee, M. L.; Healy, T. W.; White, L. R. Hydrophobicity Effects in the Condensation of Water Films on Quartz. *J. Colloid Interface Sci.* **1990**, *140* (2), 450−465.
(60) Busca, G.; Saussey, H.; Saur, O.; Lavalley, J. C.; Lorenzelli, V. Ft-Ir Characterization of the Surface-Acidity of Different Titanium-Dioxide Anatase Preparations. *Appl. Catal.* **1985**, *14* (1−3), 245−260.
(61) Herman, G. S.; Gao, Y. Growth of epitaxial anatase (001) and (101) films. *Thin Solid Films* **2001**, *397* (1−2), 157−161.
(62) Haines, W. B. Studies in the physical properties of soil, V. The hysteresis effect in capillary properties, and the modes of moisture distribution associated therewith. *J. Agric. Sci.* **1930**, *20*, 97−116.
(63) Miller, E. E.; Miller, R. D. Physical theory for capillary flow phenomena. *J. Appl. Phys.* **1956**, *4*, 324−332.
(64) Tokunaga, T.; Olson, K.; Wan, J. Conditions necessary for capillary hysteresis in porous media: Tests of grain size and surface tension influences. *Water Resour. Res.* **2004**, *40* (5), W05111.
(65) Tokunaga, T. K. Reply to Comment by Philippe Baveye on "Physicochemical controls on adsorbed water film thickness in unsaturated geological media". *Water Resour. Res.* **2012**, *48*, W11803.
(66) Klute, A.; Letey, J. The dependence of ionic diffusion on the moisture content of nonadsorbing porous media. *Soil Science Society of America Proceedings* **1958**, *22*, 213−215.
(67) Charlet, L.; Baham, J.; Giraldez, J. V.; Lo, W. C.; Aristilde, L.; Baveye, P. C. Eloge de la Methode: A tribute to Garrison Sposito on the occasion of his retirement. *Front. Environ. Sci.* **2016**, *4*, 73.

DOI: 10.1021/acs.est.6b05891
Environ. Sci. Technol. 2017, 51, 4338−4346